AMERICAN ACADEMY OF OPHTHALMOLOGY®

Widefield Choroidal Thickness of Eyes with Central Serous Chorioretinopathy Examined by Swept-Source OCT

Masaharu Ishikura, MD, Yuki Muraoka, MD, PhD, Naomi Nishigori, MD, Ayako Takahashi, MD, PhD, Masahiro Miyake, MD, PhD, Naoko Ueda-Arakawa, MD, PhD, Manabu Miyata, MD, PhD, Sotaro Ooto, MD, PhD, Akitaka Tsujikawa, MD, PhD

Purpose: To examine widefield (WF) changes in the choroidal thickness of eyes with central serous chorioretinopathy (CSC).

Design: An observational study.

Participants: Twenty-two patients (20 men and 2 women) with treatment-naïve unilateral CSC and 28 normal eyes of 28 age-matched, healthy participants (21 men and 7 women).

Methods: We performed enhanced depth imaging of swept-source (SS) OCT with a viewing angle of vertical 20 mm × horizontal 23 mm. Moreover, we developed a grid consisting of 9 subfields, with diameters of 3, 9, and 18 mm; the inner and outer rings were enclosed by circles with diameters of 3 and 9 mm and 9 and 18 mm, respectively, which were divided into 4 subfields—superotemporal, inferotemporal, superonasal, and inferonasal.

Main Outcome Measures: Widefield changes in choroidal thickness.

Results: The mean duration from the presumed onset of CSC was 6.8 ± 3.1 months during the examination. Compared with that in normal eyes, the choroidal thickness in eyes of patients with CSC was significantly greater in all subfields ($P < 0.020$ for fellow eyes; $P < 0.001$ for eyes with CSC). Compared with that in fellow eyes, the choroidal thicknesses in eyes of patients with CSC were significantly greater, except for the outer superotemporal and inferonasal subfields ($P < 0.001$ for all inner subfields; $P < 0.001$ for the outer superonasal and inferotemporal subfields). In areas with dilated vortex veins, choroidal thickening was observed from the vicinity of the vortex vein ampulla to the macula along the course of the veins. Choroidal thickening on the dominant side was significantly greater than that on the nondominant side ($P = 0.015$ for the nasal subfield of the inner ring; $P = 0.003$ and $P < 0.001$ for the temporal subfields of the inner and outer rings, respectively).

Conclusions: Enhanced depth imaging of SS-OCT facilitated the analysis of WF changes in choroidal thickness in both healthy patients and patients with CSC. The local factors of the affected vortex vein and systemic risk factors may be involved in the pathogenesis of CSC. *Ophthalmology Retina 2022;6:949-956 © 2022 by the American Academy of Ophthalmology. This is an open access article under the CC BY-NC-ND license (http://creativecommons.org/licenses/by-nc-nd/4.0/).*

Central serous chorioretinopathy (CSC) is characterized by serous retinal detachment in the posterior pole and commonly causes vision impairment in young to middle-aged persons.[1,2] Recently, CSC has been considered as a type of pachychoroid spectrum disease,[3–7] and the associated pathologic changes have attracted attention. Hyperopic refractive error, short axial length, male sex, psychological conditions, prolonged administration of corticosteroids, pregnancy, and susceptible genes are risk factors for CSC; however, researchers have not yet identified the underlying pathogenesis.[1,5,6,8–12]

Nonetheless, recent advances in OCT, particularly for the development of enhanced depth imaging (EDI), and swept-source (SS) OCT have revealed the characteristic choroidal structures of eyes with CSC.[13–21] Veins in the deep choroidal layer of an eye with CSC are more dilated, with greater subfoveal choroid thickness than in normal eyes.[21–23] However, changes in the choroidal thickness at the periphery remain controversial in CSC. Studies using anterior-segment OCT have revealed thicker sclerae in eyes with CSC than in normal eyes, thereby suggesting an association between blood flow stasis in the vortex veins penetrating the sclera and the development of CSC.[24–26] In contrast, researchers have observed choroidal thickening of eyes with CSC in the macula—but not in the periphery—using B-scan images of ultrawide field OCT.[19]

An analysis of choroidal thickness in a widefield (WF) involving the vicinity of the vortex vein ampulla may enable the exploration of the peripheral choroidal structures in eyes with CSC. Thus, we aimed to perform EDI of WF SS-OCT for healthy participants and patients with CSC and to compare the choroidal thickness maps of the corresponding areas. From these comparisons, we intended to obtain the characteristic findings suggesting the pathogenesis of typical CSC.

https://doi.org/10.1016/j.oret.2022.04.011
ISSN 2468-6530/22

Methods

Patients

This observational study was approved by the institutional review board of the Kyoto University Graduate School of Medicine (Kyoto, Japan) and adhered to the tenets of the Declaration of Helsinki. Written informed consent was obtained from each participant at the initial visit before commencing the study.

The study included eyes with treatment-naïve unilateral CSC and contralateral eyes checked at the Kyoto University Hospital between August 2021 and December 2021. The duration of symptoms from the onset was $<$ 12 months. Moreover, we included either left or right normal eyes of age-matched healthy participants as controls.

The diagnosis of CSC was based on the presence of subretinal fluid in the posterior pole, which revealed dye leakage from the retinal pigment epithelium on fluorescein angiography (FA) and focal choroidal vascular hyperpermeability on the late-phase indocyanine green angiography (ICGA). We excluded patients with other chorioretinal diseases that could accompany subretinal fluid; eyes with macular neovascularization, glaucoma, uveitis, scleritis, or ocular hypertension ($>$ 21 mmHg) or hypotension ($\leq$ 5 mmHg); and those who had received anti-VEGF treatment, intraocular or extraocular surgery other than cataract surgery, photodynamic therapy, retinal photocoagulation, or corticosteroids. Moreover, we excluded those with keratoconus, high myopia with the spherical equivalent $<$ $-$6 diopters, hyperopia $>$ +4 diopters, or astigmatism $>$ $\pm$3 diopters and pregnant women.

At the initial examination, each patient with CSC underwent an extensive ophthalmic assessment with refraction, decimal best-corrected visual acuity testing with a 5-m Landolt chart, intraocular pressure and axial length (AL), slit-lamp biomicroscopy, color fundus photography, FA, ICGA, fundus autofluorescence photography, and SS-OCT. The refraction was objectively measured using an autorefractor, and the spherical equivalent was defined as the sum of the spherical power and half of the cylinder power. We measured the AL using an interferometer (IOL Master 700; Carl Zeiss Meditec). Color fundus photography was performed using a fundus camera system (TRC50LX, Topcon Corp; 3216 $\times$ 2136 pixels). We performed FA and ICGA using a confocal scanning laser ophthalmoscope (Spectralis HRA+OCT; Heidelberg Engineering).

Evaluations of Choroidal Thickness by EDI of WF SS-OCT

We examined the choroidal structures using SS-OCT (Xephilio OCT-S1, Canon Medical Systems), with a near-infrared illumination of 1010 to 1110 nm (scanning laser ophthalmoscope, 780 nm) and a scanning speed of 100,000 A-scans per second. We set the focusing spot of OCT to 30 μm to ensure that the device could scan a large area. No additional lenses were used or device modifications were performed during image acquisition.

To measure the WF changes in choroidal thickness, we acquired 3-dimensional volume data of vertical 20 mm (128 B-scans) $\times$ horizontal 23 mm (1024 pixels) $\times$ scan depth 5.3 mm (1396 pixels) using EDI of SS-OCT. To develop *en face* SS-OCT images, we additionally acquired 3-dimensional volume data of vertical 20 mm (512 pixels) $\times$ horizontal 23 mm (512 B-scans) $\times$ scan depth 5.3 mm (1396 pixels) in a similar manner. For the segmentation of the choroid, we set the choroidal thickness as the vertical distance from the Bruch's membrane to the chorioscleral interface. The segmentation was automatically performed using built-in software supported by artificial intelligence. Automatic segmentations of the inner and outer borders of the choroid were correctly performed in normal eyes; however, they were occasionally incorrectly performed in patients with CSC. Thus, we manually corrected the segmentation errors as required.

To measure the WF choroidal thickness, we developed a grid consisting of 9 subfields comprising 3 circles with diameters of 3, 9, and 18 mm and always set the grid center on the center of the fovea (foveal bulge) without any rotation (Fig 1). The inner and outer rings were enclosed by circles with diameters of 3 and 9 mm and 9 and 18 mm, respectively. They were divided into superotemporal, inferotemporal, superonasal, and inferonasal subfields (Figs 1, 2), considering the segmental nature of the choroidal vasculature[27–29]; the venous blood in the choroid drains into its own vortex vein, and the anatomic positions of the ampullae (except for those in patients with high myopia) are usually at the equatorial areas of 4 quadrants (upper and lower temporal hemispheres and upper and lower nasal hemispheres), whereas the horizontal and vertical watersheds are between the quadrants.[18,27–29]

Using *en face* SS-OCT images of the choroid, Hiroe and Kishi[21] have recently elucidated that eyes with CSC always exhibit asymmetry in the upper and lower vortex veins. In this study, we also judged the presence or absence of asymmetry in the upper and lower vortex veins using the method implemented in the study by Hiroe and Kishi[21] (Fig 3). However, the viewing angle of the SS-OCT device used in this study was larger than that of the device used in the previous study, which involved the vicinity of the vortex vein ampulla; therefore, we slightly modified the definition as follows. Asymmetry in the upper and lower vortex veins was judged to be present if dilated vortex veins from the ampullae extended beyond the horizontal line through the fovea and involved the entire macula or the posterior pole. In contrast, asymmetry was judged to be absent if there were no distinct differences in the extent and vascular dilatation between the upper and lower vortex veins. In this study, we further identified the side (upper or lower) on which the ampulla of the dilated vortex vein was located as the dominant side and the opposite side (lower or upper) as the nondominant side. The presence of asymmetry and the dominant and nondominant sides of the vortex veins, as well as their consistencies, were evaluated for each patient with CSC via mutual agreement among 3 authors (M.I., Y.M., and N.N.). We applied the definitions of the dominant and nondominant sides on the *en face* SS-OCT images to the analyses using choroidal thickness maps.

While measuring the choroidal thickness, we unified the measurement range among participants by correcting the AL-related magnification using the modified Littmann formula (Bennett procedure).[30,31] Specifically, the AL of each participant was substituted into the Bennett formula (equation 1) so that the measured diameters (Dms) in the grid could strictly become the default diameters (Dds) of the grid.[30]

$$q = 0.01306 \times (AL - 1.82) \quad \text{(equation 1)}$$

The relationship between the Dm and Dd of the grid was computed using equation 2:

$$Dm = 1 \div (p \times q) \times Dd \quad \text{(equation 2)}$$

where p $\times$ q was the overall image magnification factor, p was the magnification factor of the imaging system (Xephilio OCT S1), and q was the magnification factor of the examined eye. The factor q was determined from equation 1, in which 1.82 is a constant related to the distance between the corneal apex and the second principal plane.[32] The factor p was computed from the Bennett formula if the AL at which the Dd was equal to the Dm was known. For the Xephilio OCT S1, the standard AL provided by the manufacturer was set as 24.20 mm. When the Dd was equal to the Dm, then p was equal to 1 / q, and p was calculated as follows: p = 1 / [0.01306 $\times$ (24.20 $-$ 1.82)] = 3.42134. The values of p and q were replaced in

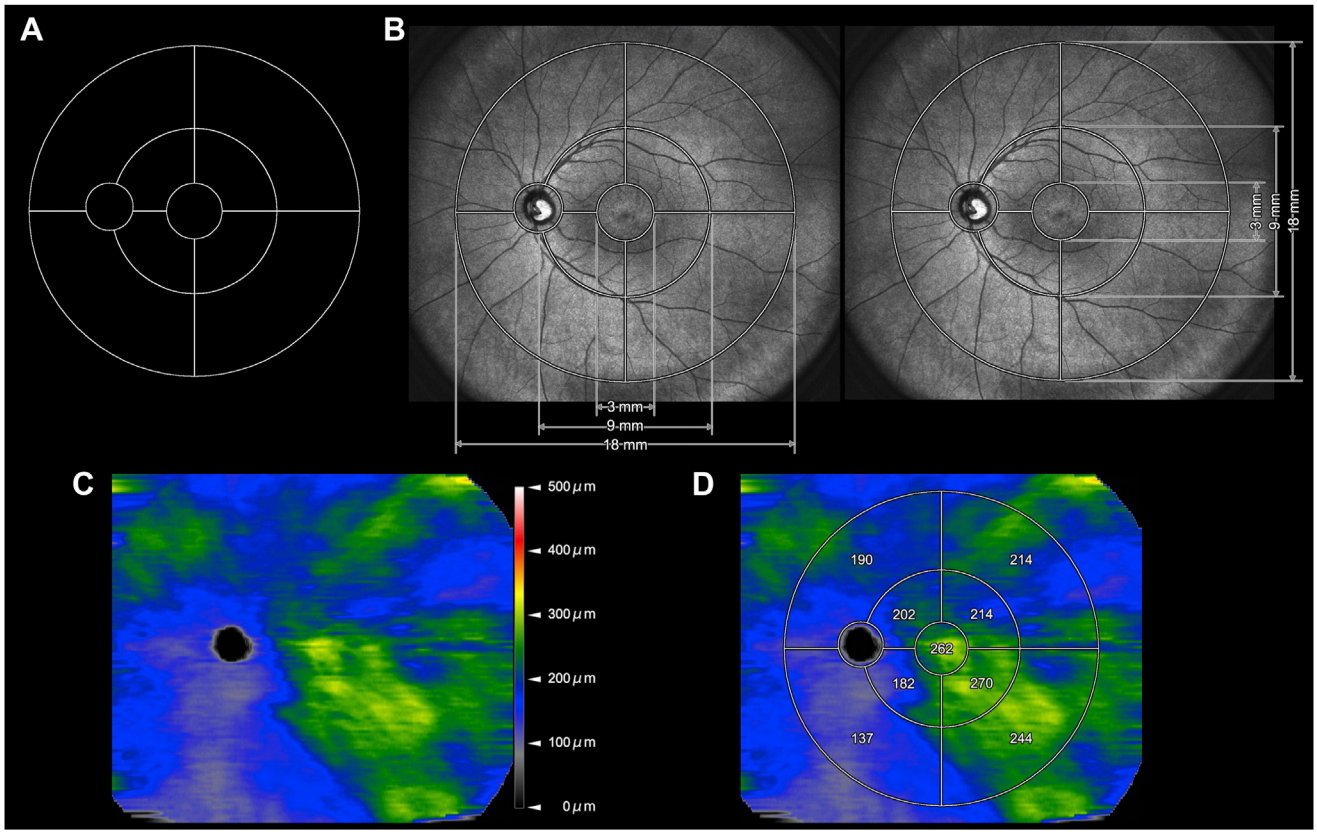

Figure 1. Thickness map analysis of the choroid using enhanced depth imaging of WF swept-source OCT. **A,** A grid was developed for measuring changes in the WF thickness in the choroid. It consisted of 9 subfields divided by 3 circles, with diameters of 3, 9, and 18 mm, and 4 lines. Circumferential and zonal areas enclosed by these circles were divided into 4 superotemporal, inferotemporal, superonasal, and inferonasal subfields, considering the arrangement of the vortex veins. **B,** Infrared scanning laser ophthalmoscopy images with the measurement grids overlaid. **C,** The WF choroidal thickness map. **D,** The WF choroidal thickness map with the grid overlaid. The value of each subfield indicates the mean choroidal thickness (μm) for the subfield. WF = widefield.

equation 2 to compute the measured size of the scan as follows: $Dm = 1 / [3.42134 \times 0.01306 \times (AL - 1.82)] \times Dd$.

Statistical Analysis

Statistical analysis was performed using PASW Statistics version 18.0 (SPSS). The values are presented as means ± standard deviations. We converted the decimal best-corrected visual acuity measured using a Landolt chart to a logarithm of the minimum angle of resolution. Comparisons between healthy participants and patients with CSC were performed using the unpaired *t* test for parameters with normal distribution and the Mann–Whitney *U* test for parameters with nonnormal distribution. For sex differences, the chi-square test was used. Comparisons between eyes with CSC and fellow eyes and those between dominant and nondominant sides of eyes with CSC were performed using the paired *t* test for parameters with normal distribution and the Wilcoxon signed rank test for parameters with nonnormal distribution. *P* values of < 0.05 were considered statistically significant.

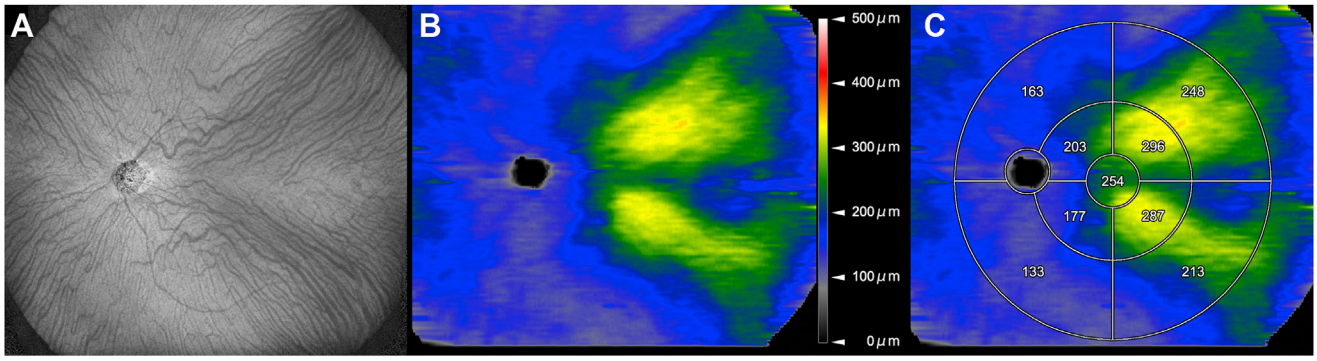

Figure 2. Widefield choroidal thickness map of a healthy participant. **A,** *En face* swept-source OCT image of the choroid. **B,** Choroidal thickness map. **C,** Choroidal thickness values measured by a grid. The value of each subfield depicts the mean choroidal thickness (μm) for the subfield.

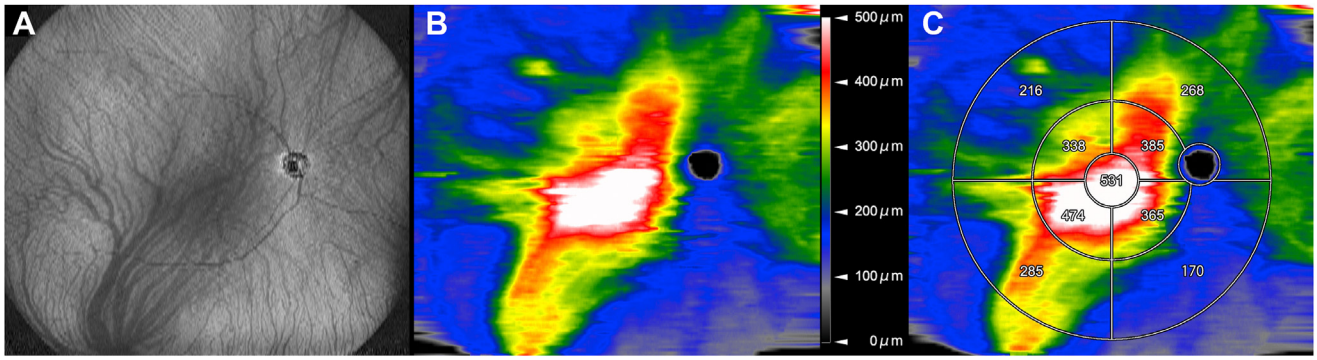

Figure 3. Widefield choroidal thickness map of an eye with central serous chorioretinopathy. **A,** *En face* swept-source OCT image of the choroid, with dilated vortex veins on the inferior side. **B,** The choroidal thickness map. **C,** The choroidal thickness measured by a grid. The value of each subfield depicts the mean choroidal thickness (μm) for the subfield. The choroidal thickening extends from the vicinity of the vortex vein ampulla at inferotemporal quadrant to the macula to the opposite superior side along the course of the vortex veins.

Results

The current study included 22 patients (20 men and 2 women) with unilateral CSC. The mean duration from the presumed onset was 6.8 ± 3.1 months during the examination. The fellow eyes did not reveal obvious OCT, FA, and fundus autofluorescense (FAF) findings suggestive of CSC during inclusion. Moreover, we examined 28 eyes of 28 age-matched, healthy participants (21 men and 7 women) as controls. All participants were Japanese. The sex, mean age, spherical equivalent and axial length were insignificantly different between the controls and the fellow and diseased eyes of patients with CSC (Table 1).

The EDI of WF SS-OCT provided choroidal thickness maps involving the vicinities of the vortex vein ampullae in both controls and patients with CSC (Figs 1–3).

Table 2 summarizes the comparisons of the WF changes in choroidal thickness between the participants. Compared with the choroidal thickness of normal eyes, those of patients with CSC were significantly greater in all subfields of the measurement grid ($P < 0.020$ for all subfields in fellow eyes; $P < 0.001$ for all subfields in eyes with CSC). The choroidal thicknesses of eyes with CSC, with the exception of the outer superotemporal and inferonasal subfields, were significantly greater than those of fellow eyes ($P < 0.001$ for all inner subfields and $P < 0.001$ for the outer superonasal and inferotemporal subfields).

The upper and lower vortex veins were vertically asymmetric in all eyes with CSC (Table 3; Fig 3). On the dominant side with dilated vortex veins, choroidal thickening was observed from the vicinity of the vortex vein ampulla to the macula along the course of the veins (Fig 3). Table 3 summarizes the comparisons of the choroidal thicknesses between the dominant and nondominant sides of eyes with CSC. The choroidal thicknesses on the dominant side were significantly greater than those on the nondominant side ($P = 0.015$ for the nasal subfield of the inner ring; $P = 0.003$ and $P < 0.001$ for temporal subfields of the inner and outer rings, respectively).

Discussion

We examined the choroidal thickness of 28 normal eyes of 28 healthy participants and 22 fellow and diseased eyes of patients with unilateral CSC using EDI of WF SS-OCT.

OCT is an essential imaging modality for the diagnosis and management of chorioretinal diseases. In addition to OCT B-scans, the analysis of thickness maps is clinically useful. A thickness map of the inner retina is useful for diagnosing glaucoma or detecting areas of retinal ischemia, whereas that of the entire retinal layer is useful for monitoring pathologic conditions, such as macular edema.[33,34] The development of a retinal thickness map is relatively easier in the absence of marked retinal hemorrhage or edema. In contrast, the development of a choroidal thickness map is challenging because the retinal pigment epithelium and choroid contain large amounts of melanin pigment, thus making it difficult to obtain sufficient OCT signals from the choroid.

However, the development of EDI and the advent of SS-OCT with penetrative beams have enabled the evaluation of choroidal structures.[15,16,19,24,35] Recent investigations with EDI and SS-OCT have elucidated that eyes with CSC have thicker subfoveal choroid and that the veins are prominently dilated in the deep choroidal layer (Haller's layer).[8,21–23,25,36] However, most of the previous examinations only evaluated the macular area, whereas pathologic changes at the periphery have not been sufficiently investigated. The imaging modality and protocol adopted in this study (EDI of WF SS-OCT) helped us measure the choroidal thickness involving the vicinity of the vortex vein ampulla in both healthy participants and patients with CSC (Figs 1–3). To our knowledge, no reports have extensively examined the choroidal structure using a high-quality thickness map. Using ultra-WF OCT B-scans, Izumi et al[19] observed greater subfoveal choroidal thickness in eyes with CSC than in normal eyes; however, the thickness was insignificantly different in the periphery, contrary to our results. This may be attributed to the fact that their analysis was based on OCT B-scans.[19]

For valid measurements of WF choroidal thickness, we developed a grid consisting of 9 subfields. The grid center was always set on the center of the fovea without any rotation (Fig 1). However, differences in the ALs among subjects can generally affect the choroidal thickness and the measurement range within the grid.[30,32] In this study, we unified the measurement range among participants by correcting the

Table 1. Characteristics of Healthy Subjects and Patients with Central Serous Chorioretinopathy

Clinical Parameters	Healthy Subjects	Patients with CSC	*P* Value
No. (men/women)	28 (21/7)	22 (20/2)	0.15*
No. of eyes	28	22	NA
Age (yrs)	57.4 ± 16.1	52.4 ± 12.0	0.21†
Systolic BP (mmHg)	125 ± 14	130 ± 13	0.21‡
Diastolic BP (mmHg)	78 ± 8	82 ± 7	0.14‡
Duration of symptoms (mos)	NA	6.8 ± 3.1	NA

		Fellow eyes	Diseased eyes	*P* value§	*P* value‖	*P* value¶
Spherical equivalent (diopters)	−1.6 ± 3.3	−1.7 ± 2.7	−1.4 ± 2.8	0.49†	0.88†	0.72#
Axial length (mm)	24.4 ± 1.3	24.13 ± 1.1	23.8 ± 1.2	0.90†	0.36†	0.25#
LogMAR visual acuity	−0.1 ± 0.1	0.0 ± 0.2	0.0 ± 0.2	0.89†	0.64†	0.58#
Snellen visual acuity (range)	20/25 to 20/13	20/25 to 20/13	20/50 to 20/13	NA		
Intraocular pressure (mmHg)	15.6 ± 3.1	14.2 ± 2.4	14.7 ± 2.8	0.12‡	0.28‡	0.45**

BP = blood pressure; CSC = central serous chorioretinopathy; logMAR = logarithm of the minimum angle of resolution; NA = not applicable,
Data are presented as means ± standard deviations unless otherwise indicated.
*Comparisons of systemic factors between healthy participants and patients with CSC were performed using the chi-square test for sex differences.
†Comparisons of systemic factors between healthy participants and patients with CSC were performed using Mann−Whitney U test for parameters with nonnormal distribution.
‡Comparisons of systemic factors between healthy participants and patients with CSC were performed using unpaired *t* test for parameters with normal distribution.
§Comparisons of ocular factors between healthy eyes and fellow eyes of patients with CSC were performed using the unpaired *t* test for parameters with normal distribution and using the Mann−Whitney *U* test for parameters with nonnormal distribution.
‖Comparisons of ocular factors between healthy eyes and eyes of patients with CSC were performed using the unpaired *t* test for parameters with normal distribution and using the Mann−Whitney *U* test for parameters with nonnormal distribution.
¶Comparisons of ocular factors between fellow and diseased eyes of patients with CSC were performed using the paired *t* test for parameters with normal distribution and using the Wilcoxon signed rank test for parameters with nonnormal distribution.
#Comparisons of ocular factors between fellow and diseased eyes of patients with CSC were performed using the Wilcoxon signed-rank test for parameters with nonnormal distribution.
**Comparisons of ocular factors between fellow and diseased eyes of patients with CSC were performed using the paired t-test for parameters with normal distribution.

AL-related magnification based on a previous report.[30] In addition, we confirmed that there were no significant differences in the ALs between the healthy participants and patients with CSC and between the fellow and diseased eyes of patients with CSC (Table 1). We believe that the inclusion and exclusion criteria, correction for the AL-related magnification, and strict determination of the foveal center on the grid enabled valid measurements of choroidal thickness with the minimum possible bias. Compared with normal eyes, those with CSC had significantly thicker choroid in all subfields ($P < 0.001$ for all; Table 2; Fig 3). In other words, choroidal thickening in eyes with CSC was not limited to the subfoveal membrane but extended to the periphery. We observed a significant difference between the normal eyes and fellow eyes of the patients (Table 2), thus suggesting that patients with CSC have some systemic risk factors that are absent in healthy individuals.

Interestingly, differences in choroidal thickness were visible in the comparisons between the fellow and diseased eyes of the patients (Table 2; Figs 2, 3) and those between the dominant and nondominant sides of identical eyes with CSC (Table 3; Fig 3). Thus, local factors of the affected eye may also exert an effect on the development of CSC. Vertically asymmetric and dilated vortex veins, geographic filling delay on ICGA, and the remodeling of vortex veins in the watershed zone are associated with CSC pathologies.[17,18,21,22,37] Studies using anterior-segment OCT have demonstrated that the sclerae might be thicker in eyes of patients with CSC than in normal eyes and thicker in eyes of patients with CSC with fluid loculation than in eyes of those without fluid loculation.[24–26] In this study, dilated vortex veins on the dominant side displayed choroidal thickening from the vicinity of the vortex vein ampulla to the macula along the course of the veins (Fig 3; Tables 2, 3). Our current findings may support the recent understanding of the pathogenesis of typical CSC, which supposedly involves congestion due to the impaired drainage of the affected vortex veins.[1,17,18,21,22,38]

This study has several limitations. First, we included CSC with an onset of < 12 months; however, it was challenging to precisely determine the duration of onset. Second, we used SS-OCT with a viewing angle of vertical 20 mm × horizontal 23 mm; however, the vortex vein ampullae could not be simultaneously captured in the 4 quadrants with this viewing angle. Third, the distortion of WF SS-OCT was conceivable, particularly at the periphery. In addition, the measurement was performed obliquely to the chorioscleral interface at the periphery, compared with the macula. Thus, we speculated that the choroidal thickness may have been easily overestimated at the periphery. However, the possible bias in the measurement of the choroidal thickness at the periphery was not sufficiently large to distort our results and conclusions

Table 2. Comparisons of Choroidal Thickness in the Posterior Poles between Healthy Subjects and Patients with Central Serous Chorioretinopathy

Choroidal Thickness (μm)	Healthy Subjects	Patients with CSC		P Value*	P Value†	P Value‡
		Fellow Eyes	*Diseased Eyes*			
Central subfield (3 mm)	263 ± 96	348 ± 108	420 ± 124	0.006	< 0.001	< 0.001
Subfields (3–9 mm)						
Superonasal	238 ± 80	301 ± 95	355 ± 117	0.014	< 0.001	< 0.001
Inferonasal	200 ± 77	262 ± 91	324 ± 112	0.018	< 0.001	< 0.001
Superotemporal	264 ± 65	329 ± 96	369 ± 95	0.009	< 0.001	< 0.001
Inferotemporal	243 ± 69	336 ± 90	395 ± 108	< 0.001	< 0.001	0.001
Subfields (9–18 mm)						
Superonasal	202 ± 59	262 ± 83	282 ± 92	0.004	< 0.001	< 0.001
Inferonasal	154 ± 43	189 ± 57	202 ± 62	0.012	< 0.001	0.179
Superotemporal	225 ± 47	279 ± 71	292 ± 68	0.006	< 0.001	0.076
Inferotemporal	186 ± 37	249 ± 51	279 ± 73	< 0.001	< 0.001	< 0.001

CSC = central serous chorioretinopathy.
Data are presented as means ± standard deviations unless otherwise indicated.
*Comparisons between healthy eyes and fellow eyes of patients with CSC were performed using the Mann–Whitney *U* test.
†Comparisons between healthy eyes and eyes of patients with CSC were performed using the Mann–Whitney *U* test.
‡Comparisons between fellow and diseased eyes of patients with CSC were performed using the Wilcoxon signed rank test.

because of no significant between-group differences in the background ocular and systemic factors. In addition, we made some comparisons between identical patients or eyes. Fourth, we determined the dominant and nondominant sides based on previously reported methods, which were easy but subjective.[17]

Despite the aforementioned limitations, our results using EDI of WF SS-OCT may provide evidence for the involvement of blood flow stasis or overload in the affected vortex vein in the pathogenesis of CSC. The imaging protocol used in this study will facilitate the elucidation of the physiology of the choroidal circulation and pathologies of chronic or atypical CSC and other pachychoroid spectrum diseases.

Table 3. Comparisons of Choroidal Thickness between Dominant and Nondominant Sides of Eyes with Central Serous Chorioretinopathy

Choroidal Thickness (μm)	Dominant Side	Nondominant Side	P Value
Nasal			
Subfields (3–9 mm)	350 ± 116	329 ± 114	0.015
Subfields (9–18 mm)	254 ± 84	230 ± 90	0.070
Temporal			
Subfields (3–9 mm)	397 ± 99	367 ± 104	0.003
Subfields (9–18 mm)	304 ± 67	268 ± 70	< 0.001

Data are presented as mean ± standard deviation unless otherwise indicated. The choroidal thickness of the dominant and nondominant sides was compared using the Wilcoxon signed rank test.

Footnotes and Disclosures

Originally received: January 8, 2022.
Final revision: March 31, 2022.
Accepted: April 11, 2022.
Available online: April 15, 2022. Manuscript no. ORET-D-22-00014R1.

Department of Ophthalmology and Visual Sciences, Kyoto University Graduate School of Medicine, Kyoto, Japan.

Disclosure(s):

All authors have completed and submitted the ICMJE disclosures form.

The author(s) made the following disclosure(s): Y.M.: Honoraria — Bayer Yakuhin, Novartis Pharma, Canon, Alcon Japan, Santen Pharmaceutical, Senju Pharmaceutical, AMO Japan.

A.T.: Honoraria — Bayer Yakuhin, Novartis Pharma, Findex.

M.Miyake.: Honoraria — Novartis Pharma, Bayer Yakuhin, Kowa Pharmaceutical, Nitten Pharmaceutical, Alcon Japan, HOYA, NEVAKAR INC, AMO Japan, Santen Pharmaceutical, Ellex, Senju Pharmaceutical, Johnson & Johnson KK.

M.Miyata: Honoraria — Alcon Japan, Novartis Pharma, Santen Pharmaceutical, HOYA, Bayer Yakuhin; Sotaro Ooto: Bayer Yakuhin, Kowa Pharmaceutical, Alcon Pharma, Janssen Pharmaceutical, Novartis Pharma, AMO Japan, Santen Pharmaceutical, Alcon Japan, Senju Pharmaceutical, Japan Focus.

S.O.: Honoraria — Bayer Yakuhin, Kowa Pharmaceutical, Alcon Pharma, Janssen Pharmaceutical, Novartis Pharma, AMO Japan, Santen Pharmaceutical, Alcon Japan, Senju Pharmaceutical, Japan Focus.

A.T.: Honoraria — Canon, Findex, Santen Pharmaceutical, Kowa Pharmaceutical, Pfizer, AMO Japan, Senju Pharmaceutical, Wakamoto Pharmaceutical, Alcon Japan, Alcon Pharma, Otsuka Pharmaceutical, Tomey Corporation, Taiho Pharma, HOYA, Bayer Yakuhin, Novartis Pharma, Chugai Pharmaceutical, Astellas, Eisai, Daiich-Sankyo, Janssen Pharmaceutical, Kyoto Drug Discovery & Development, Allergan Japan, MSD, Ellex, Sanwa Kagaku Kenkyusho, Nitten Pharmaceutical, AbbVie GK.

Supported in part by a grant-in-aid for scientific research (no. 20K09771) from the Japan Society for the Promotion of Science (Tokyo, Japan) and Canon Inc. (Tokyo, Japan). These organizations had no role in the design or conduct of this research. The funders had no role in the study design, data collection and analysis, the decision to publish, or the preparation of the manuscript.

HUMAN SUBJECTS: Human subjects were included in this study.

This observational study was approved by the institutional review board of the Kyoto University Graduate School of Medicine (Kyoto, Japan) and adhered to the tenets of the Declaration of Helsinki. Written informed consent was obtained from each participant at the initial visit before commencing the study.

No animal subjects were used in this study.

Author Contributions:

Conception and design: Muraoka

Data collection: Ishikura, Muraoka, Nishigori, Takahashi, Miyake

Analysis and interpretation: Ishikura, Muraoka, Nishigori, Ueda-Arakawa, Miyata, Ooto, Tsujikawa

Obtained funding: N/A

Overall responsibility: Ishikura, Muraoka

Abbreviations and Acronyms:
AL = axial length; **CSC** = central serous chorioretinopathy; **Dd** = default diameter; **Dm** = measured diameter; **EDI** = enhanced depth imaging; **FA** = fluorescein angiography; **ICGA** = indocyanine green angiography; **SS** = swept-source; **WF** = widefield.

Keywords:
Central serous chorioretinopathy (CSC), Enhanced depth imaging (EDI), Swept-source optical coherence tomography (SS-OCT), Widefield (WF).

Correspondence:
Yuki Muraoka, MD, PhD, Department of Ophthalmology, Kyoto University Graduate School of Medicine, Sakyo-ku, Kyoto 606-8507, Japan. E-mail: muraoka@kuhp.kyoto-u.ac.jp.

References

1. Daruich A, Matet A, Dirani A, et al. Central serous chorioretinopathy: recent findings and new physiopathology hypothesis. *Prog Retin Eye Res*. 2015;48:82−118.
2. Kido A, Miyake M, Tamura H, et al. Incidence of central serous chorioretinopathy (2011-2018): a nationwide population-based cohort study of Japan. Br J Ophthalmol. In press.
3. Miyake M, Ooto S, Yamashiro K, et al. Pachychoroid neovasculopathy and age-related macular degeneration. *Sci Rep*. 2015;5:16204.
4. Pang CE, Freund KB. Pachychoroid neovasculopathy. *Retina*. 2015;35:1−9.
5. Hosoda Y, Yoshikawa M, Miyake M, et al. *CFH* and *VIPR2* as susceptibility loci in choroidal thickness and pachychoroid disease central serous chorioretinopathy. *Proc Natl Acad Sci U S A*. 2018;115:6261−6266.
6. Hosoda Y, Miyake M, Schellevis RL, et al. Genome-wide association analyses identify two susceptibility loci for pachychoroid disease central serous chorioretinopathy. *Commun Biol*. 2019;2:468.
7. Siedlecki J, Schworm B, Priglinger SG. The pachychoroid disease spectrum-and the need for a uniform classification system. *Ophthalmol Retina*. 2019;3:1013−1015.
8. Kaye R, Chandra S, Sheth J, et al. Central serous chorioretinopathy: an update on risk factors, pathophysiology and imaging modalities. *Prog Retin Eye Res*. 2020;79:100865.
9. Yannuzzi LA. Type A behavior and central serous chorioretinopathy. *Retina*. 2012;32(suppl 1):709.
10. Honda S, Miki A, Kusuhara S, et al. Choroidal thickness of central serous chorioretinopathy secondary to corticosteroid use. *Retina*. 2017;37:1562−1567.
11. Azad AD, Zhou M, Afshar AR, et al. Systemic corticosteroid use after central serous chorioretinopathy diagnosis. *Ophthalmology*. 2021;128:121−129.
12. Miki A, Sakurada Y, Tanaka K, et al. Genome-wide association study to identify a new susceptibility locus for central serous chorioretinopathy in the Japanese population. *Invest Ophthalmol Vis Sci*. 2018;59:5542−5547.
13. Spaide RF, Koizumi H, Pozzoni MC. Enhanced depth imaging spectral-domain optical coherence tomography. *Am J Ophthalmol*. 2008;146:496−500.
14. Wong IY, Koizumi H, Lai WW. Enhanced depth imaging optical coherence tomography. *Ophthalmic Surg Lasers Imaging*. 2011;42(suppl):S75−S84.
15. Jirarattanasopa P, Ooto S, Tsujikawa A, et al. Assessment of macular choroidal thickness by optical coherence tomography and angiographic changes in central serous chorioretinopathy. *Ophthalmology*. 2012;119:1666−1678.
16. Suzuki M, Gomi F, Hara C, et al. Characteristics of central serous chorioretinopathy complicated by focal choroidal excavation. *Retina*. 2014;34:1216−1222.
17. Kishi S, Matsumoto H, Sonoda S, et al. Geographic filling delay of the choriocapillaris in the region of dilated asymmetric vortex veins in central serous chorioretinopathy. *PLoS One*. 2018;13:e0206646.
18. Matsumoto H, Hoshino J, Mukai R, et al. Vortex vein anastomosis at the watershed in pachychoroid spectrum diseases. *Ophthalmol Retina*. 2020;4:938−945.
19. Izumi T, Maruko I, Kawano T, et al. Morphological differences of choroid in central serous chorioretinopathy determined by ultra-widefield optical coherence tomography. *Graefes Arch Clin Exp Ophthalmol*. 2022;260:295−301.
20. Fujita A, Aoyama Y, Tsuneyoshi S, et al. Association between visual function and the integrity of residual ellipsoid zone in resolved central serous chorioretinopathy. *Sci Rep*. 2019;9:12433.
21. Hiroe T, Kishi S. Dilatation of asymmetric vortex vein in central serous chorioretinopathy. *Ophthalmol Retina*. 2018;2:152−161.
22. Spaide RF, Gemmy Cheung CM, Matsumoto H, et al. Venous overload choroidopathy: a hypothetical framework for central serous chorioretinopathy and allied disorders. *Prog Retin Eye Res*. 2022;86:100973.
23. Chen G, Tzekov R, Li W, et al. Subfoveal choroidal thickness in central serous chorioretinopathy: a meta-analysis. *PLoS One*. 2017;12:e0169152.
24. Imanaga N, Terao N, Nakamine S, et al. Scleral thickness in central serous chorioretinopathy. *Ophthalmol Retina*. 2021;5:285−291.
25. Imanaga N, Terao N, Sawaguchi S, et al. Clinical factors related to loculation of fluid in central serous chorioretinopathy. *Am J Ophthalmol*. 2022;235:197−203.
26. Terao N, Imanaga N, Wakugawa S, et al. Ciliochoroidal effusion in central serous chorioretinopathy. *Retina*. 2022;42:730−737.
27. Hayreh SS. Segmental nature of the choroidal vasculature. *Br J Ophthalmol*. 1975;59:631−648.
28. Hayreh SS. In vivo choroidal circulation and its watershed zones. *Eye (Lond)*. 1990;4:273−289.
29. Kutoglu T, Yalcin B, Kocabiyik N, Ozan H. Vortex veins: anatomic investigations on human eyes. *Clin Anat*. 2005;18:269−273.
30. Bennett AG, Rudnicka AR, Edgar DF. Improvements on Littmann's method of determining the size of retinal features by fundus photography. *Graefes Arch Clin Exp Ophthalmol*. 1994;232:361−367.
31. Kadomoto S, Muraoka Y, Ooto S, et al. Evaluation of macular ischemia in eyes with branch retinal vein occlusion: an optical

coherence tomography angiography study. *Retina*. 2018;38:272–282.
32. Flores-Moreno I, Lugo F, Duker JS, Ruiz-Moreno JM. The relationship between axial length and choroidal thickness in eyes with high myopia. *Am J Ophthalmol*. 2013;155:314–319.e1.
33. Lee WJ, Kim TJ, Kim YK, et al. Serial combined wide-field optical coherence tomography maps for detection of early glaucomatous structural progression. *JAMA Ophthalmol*. 2018;136:1121–1217.
34. Loduca AL, Zhang C, Zelkha R, Shahidi M. Thickness mapping of retinal layers by spectral-domain optical coherence tomography. *Am J Ophthalmol*. 2010;150:849–855.
35. Chung H, Byeon SH, Freund KB. Focal choroidal excavation and its association with pachychoroid spectrum disorders: a review of the literature and multimodal imaging findings. *Retina*. 2017;37:199–221.
36. Gattoussi S, Freund KB. Multimodal imaging in central serous chorioretinopathy. *Ophthalmology*. 2017;124:1331.
37. Matsumoto H, Kishi S, Mukai R, Akiyama H. Remodeling of macular vortex veins in pachychoroid neovasculopathy. *Sci Rep*. 2019;9:14689.
38. Matsumoto H, Hoshino J, Arai Y, et al. Quantitative measures of vortex veins in the posterior pole in eyes with pachychoroid spectrum diseases. *Sci Rep*. 2020;10:19505.

Pictures & Perspectives

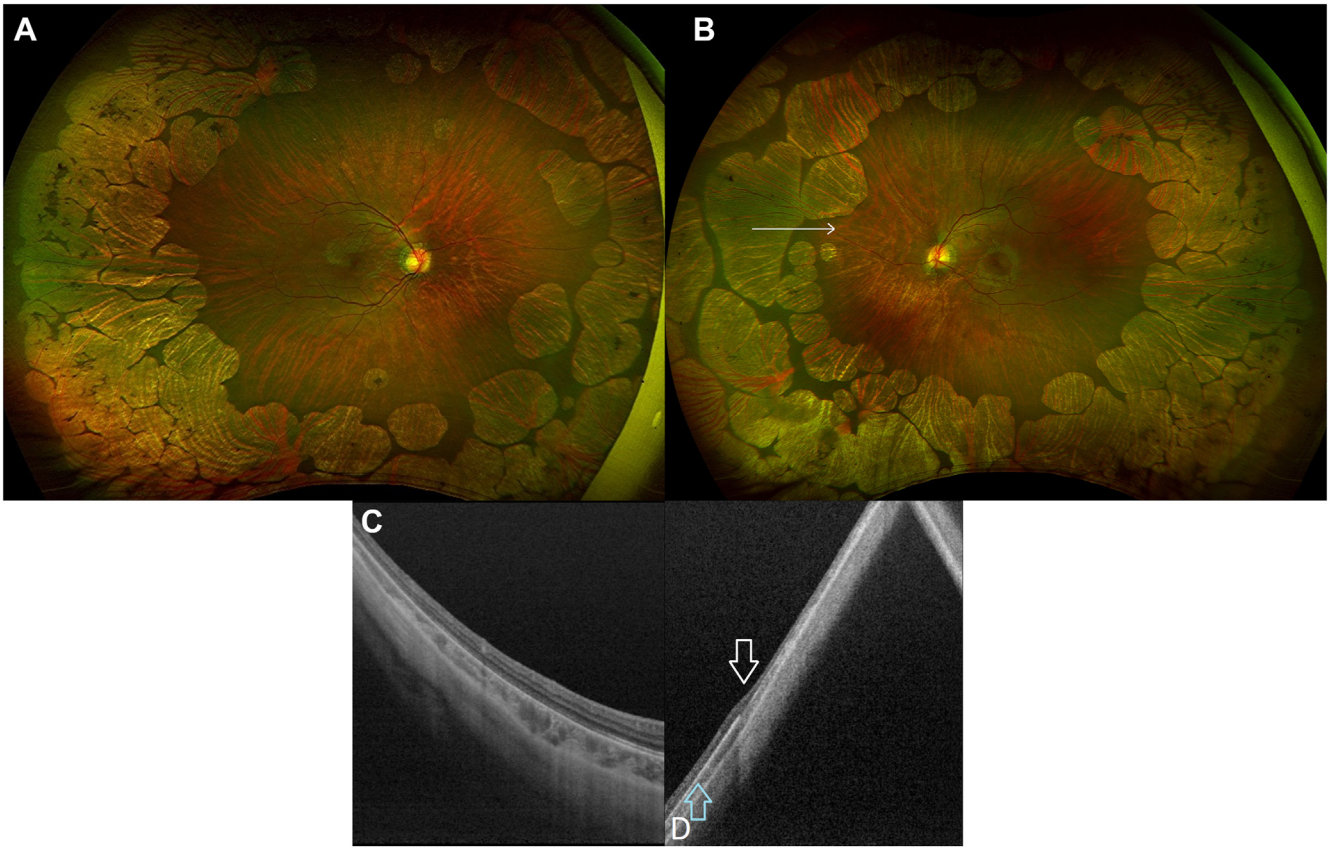

Ultrawide-field OCT in Gyrate Atrophy

An ultrawide-field OCT (Optos Silverstone SS-OCT, Nikon) performed on a 20-year-old female patient with high myopia and gyrate atrophy (Fig **A**–**D**) showed nonatrophic retina area (Fig **C**) and the junction of normal and "atrophic" retina (Fig **B**, scan vector; Fig **D**, white arrow) with sharp discontinuation of the ellipsoid line, thinning of the inner and outer retina corresponding to atrophy of photoreceptors, retinal pigment epithelium, and choroidal layers. Directly adjacent to the atrophic areas, photoreceptor atrophy with underlying hyperplastic retinal pigment epithelium (blue arrow) can be seen in (Fig **D**), compared with (Fig **C**) (Magnified version of Fig **A**-**D** is available online at www.ophthalmologyretina.org).

Inderjeet Kaur, MD
Amber Amar Bhayana, MD
Hemant Kumar Joshi, MOptom
Dr. Rajendra Prasad Centre for Ophthalmic Sciences, All India Institute of Medical Sciences, New Delhi, India